Available online at www.sciencedirect.com
SCIENCE DIRECT®
ELSEVIER
Nuclear Instruments and Methods in Physics Research A 538 (2005) 45–64
NUCLEAR INSTRUMENTS & METHODS IN PHYSICS RESEARCH Section A
www.elsevier.com/locate/nima

Surface superconductivity in niobium for superconducting RF cavities

S. Casalbuoni[a,b,*], E.A. Knabbe[b], J. Kötzler[a], L. Lilje[b], L. von Sawilski[a], P. Schmüser[c], B. Steffen[b,c]

[a]*Institut für Angewandte Physik, Universität Hamburg, Jungiusstrasse 11, D-20355 Hamburg, Germany*
[b]*DESY, Notkestrasse 85, D-22607 Hamburg, Germany*
[c]*Institut für Experimental Physik, Universität Hamburg, Notkestrasse 85, D-22607 Hamburg, Germany*

Received 25 May 2004; received in revised form 27 August 2004; accepted 6 September 2004
Available online 5 October 2004

Abstract

A systematic study is presented on the superconductivity (SC) parameters of the ultrapure niobium used for the fabrication of the nine-cell 1.3 GHz cavities for the linear collider project TESLA. Cylindrical Nb samples have been subjected to the same surface treatments that are applied to the TESLA cavities: buffered chemical polishing (BCP), electrolytic polishing (EP), low-temperature bakeout (LTB). The magnetization curves and the complex magnetic susceptibility have been measured over a wide range of temperatures and DC magnetic fields, and also for different frequencies of the applied AC magnetic field. The bulk superconductivity parameters such as the critical temperature $T_c = 9.26$ K and the upper critical field $B_{c2}(0) = 410$ mT are found to be in good agreement with previous data. Evidence for surface superconductivity at fields above B_{c2} is found in all samples. The critical surface field exceeds the Ginzburg–Landau field $B_{c3} = 1.695 B_{c2}$ by about 10% in BCP-treated samples and increases even further if EP or LTB are applied. From the field dependence of the susceptibility and a power-law analysis of the complex AC conductivity and resistivity the existence of two different phases of surface superconductivity can be established which resemble the Meissner and Abrikosov phases in the bulk: (1) "coherent surface superconductivity", allowing SC shielding currents flowing around the entire cylindrical sample, for external fields B in the range $B_{c2} < B < B_{c3}^{coh}$, and (2) "incoherent surface superconductivity" with disconnected SC domains for $B_{c3}^{coh} < B < B_{c3}$. The "coherent" critical surface field separating the two phases is found to be $B_{c3}^{coh} = 0.81\, B_{c3}$ for all samples. The exponents in the power law analysis are different for BCP and EP samples, pointing to different surface topologies.

PACS: 74.25.Nf; 74.25.Dw; 74.25.Op; 74.25.Sv; 81.65.Mq; 81.65.Cf; 84.90.+a; 85.25.Dq

Keywords: Surface superconductivity; Niobium; Phase transitions; Critical exponents; Magnetic susceptibility; Superconducting RF cavities

*Corresponding author. DESY, Notkestrasse 85, D-22607 Hamburg, Germany. Tel.: +49 40 8998 3012; fax: +49 40 8998 3282.
E-mail address: Sara.Casalbuoni@desy.de (S. Casalbuoni).

0168-9002/$ - see front matter © 2004 Elsevier B.V. All rights reserved.
doi:10.1016/j.nima.2004.09.003

1. Introduction

The proposed linear electron–positron collider project TESLA is based on superconductor technology for particle acceleration. For a centre-of-mass energy of 500 GeV (TESLA 500) an accelerating field of 23.4 MV/m is required in the 1.3 GHz nine-cell cavities which are made from pure niobium and cooled by superfluid helium at 2 K. The cavities for the TESLA Test Facility (TTF) linac are fabricated from 2.8 mm thick niobium sheets by deep drawing and electron beam welding. A damage layer of about 150 μm thickness is removed from the inner surface to obtain optimum performance in the superconducting state. For the TTF cavities this has been done so far by chemical etching which consists of two alternating processes: dissolution of the natural Nb_2O_5 layer by HF and re-oxidation of the niobium by a strongly oxidizing acid such as nitric acid (HNO_3) [1,2]. To reduce the etching speed a buffer substance is added, for example phosphoric acid, and the mixture is cooled below 15 °C. The standard procedure with a removal rate of about 1 μm per minute is called buffered chemical polishing (BCP) using an acid mixture of HF (40%), HNO_3 (65%) and H_3PO_4 (85%) in a volume ratio of 1:1:2. In the most recent industrial production of 24 TTF cavities an average gradient 26.1 ± 2.3 MV/m at a quality factor $Q_0 = 1 \times 10^{10}$ was achieved. The technology developed for TTF is hence adequate for TESLA 500 but considerable improvements are needed for an upgrade of the collider to 800 GeV (TESLA 800). A detailed description of the present status of the nine-cell cavity layout, fabrication, preparation and tests can be found in [3].

After many years of intensive R&D there exists now compelling evidence that the BCP process limits the attainable field in multi-cell niobium cavities to about 30 MV/m. This is significantly below the physical limit of about 45 MV/m which is given by the condition that the radio frequency (RF) magnetic field has to stay below the critical field of the superconductor, which for the type II superconductor niobium appears to be close to the thermodynamic critical field ($B_c \approx 190$ mT at 2 K).

An alternative surface preparation method is electrolytic polishing (EP). The material is removed in an acid mixture (for example HF and H_2SO_4) under the flow of an electric current. Sharp edges or tips are smoothed out and a very glossy surface can be obtained. Using electrolytic polishing, scientists at the KEK laboratory in Tsukuba (Japan) achieved gradients of up to 40 MV/m in single-cell cavities [4,5]. Meanwhile gradients of 35–40 MV/m have been obtained repeatedly in many 1.3 GHz single-cell test cavities [6–8]. Recently the EP technology has been successfully transferred to the nine-cell TESLA cavities yielding a record value of 39 MV/m in a multicell cavity [9].

The superiority of EP as compared to BCP can be partially understood in terms of the much reduced surface roughness. The sharp ridges at the grain boundaries of an etched niobium surface may cause local enhancements of the RF magnetic field and thereby lead to a premature breakdown of superconductivity at these localized spots. A model based on this idea, developed by Knobloch et al. [10], is able to explain the reduction of the quality factor at high field. However, a puzzling observation which does not fit into this geometrical picture was made during the CERN-DESY-Saclay R&D programme on the electropolishing of single-cell cavities [8]: after the EP and rinsing with ultrapure water the cavities failed to reach full performance but exhibited a strong decrease of quality factor when high fields were approached. Applying a 24–48 h "bakeout" at 120–140 °C to the evacuated cavity resulted in a dramatic improvement: very high gradients were accessible and the "Q drop" vanished. It should be noted that the EP treatment at KEK [4,5] already included a bakeout at 85 °C. The BCS surface resistance at 1.3–1.5 GHz is found to be reduced by a factor of 2 after baking [8,11]. However, by removing a layer of ~200–300 nm in steps of ~50 nm from the EP surface by "oxipolishing" the reduction in R_{BCS} is lost and the "Q drop" reappears [11]. The reduction of R_{BCS} during baking has been attributed to oxygen atoms diffusing either from the dielectric Nb_2O_5 layer or from intergrain niobium oxides/suboxides down to a depth of 200–300 nm [11]. For further

discussions we refer to the review talks by Kneisel [12] and Visentin [13] at the SRF2003 Workshop. Relevant investigations on the influence of surface treatment on single cell cavities have been presented at the same workshop by Ciovati et al. [14].

Another explanation for the superiority of electropolished cavities has been proposed by Halbritter [15]. The smoother surface of an EP-treated cavity with diminished grain boundary etching may lead to a reduction of dielectric surface losses which are caused by interface tunnel exchange between the conduction electrons in Nb and localized states in the Nb–Nb_2O_{5-x} interface.

Magnetic measurements on niobium samples are a useful tool to explore the surface treatments which improve cavity performance. This idea is based on the fact that for pure niobium the ratio $\kappa = \lambda_L/\xi$ is in the order of unity, so that surface superconductivity and electromagnetic losses of microwave fields reside in thin surface sheaths of nearly the same thickness, given by the correlation length ξ and the penetration depth λ_L, respectively. The experimental studies on the magnetization and susceptibility of niobium samples presented here have been carried out with the aim to gain an understanding of the superconducting properties in this sheath and their dependence on the various treatments (BCP, EP, bakeout) that are applied to the TESLA cavities. The samples have been cut from remainders of the niobium sheets used in cavity production and have been subjected to the same chemical, electro-chemical and thermal treatments as the TESLA cavities.

2. Experimental procedure

The samples for the magnetization and susceptibility measurements are cylinders with a raw diameter of 2.5 mm and a height of 2.8 mm which are cut by electro-erosion from the Nb sheets used for RF cavity production. The niobium is of high purity with a residual resistivity ratio *RRR* of 300. The impurity contents is given in Table 1. The electroerosion leaves an oxide surface layer of several μm thickness which is removed by chemical etching of about 50 μm, applying the standard BCP process. The samples are rinsed with ultra-

Table 1
Impurity contents ppm (per weight) of the Nb samples

Ta	210–950 ppm	O	< 40 ppm
W	< 100 ppm	N	< 20 ppm
Mo	< 50 ppm	C	< 20 ppm
Ti	< 40 ppm	H	< 3 ppm
Fe	< 30 ppm		

pure water and annealed for 2 h at 800 °C in a vacuum furnace ($p < 10^{-7}$ mbar) to remove dissolved hydrogen and relieve mechanical stress in the material. After the annealing a second 50 μm BCP and water rinsing is applied. In this state the samples have a similar surface structure as the BCP-treated cavities.

Several samples have been electropolished after the BCP treatment. Only the cylindrical surface has been polished with a removed thickness between 40 and 165 μm. The EP has been carried out at room temperature in a mixture of HF (56%) and H_2SO_4 (90%). Low temperature baking (LTB) has been applied both to BCP- and EP-treated samples, with a bakeout temperature of 100 ± 1 °C, 120 ± 5 °C, 123 ± 1 °C resp. 144 ± 1 °C and a baking time between 12 and 96 h in a vacuum furnace at $p < 10^{-7}$ mbar. Three of the BCP-treated and baked samples have been subsequently etched by 1, 5 and 10 μm in order to investigate whether possible baking effects are lost by the removal of the surface layer.

Scanning electron microscopy and atomic force microscopy [16] reveal a very low surface roughness of about 1 nm on the Nb grains (area of about $10 \times 10\,\mu m^2$). The steps at grain boundaries are in the order of few μm on BCP-treated samples and below 0.1 μm after the EP [17].

The sample magnetization is determined with a commercial SQUID magnetometer (Quantum Design $MPMS_2$) at temperatures ranging from 2 to 300 K in external DC fields between zero and 1 Tesla (see Appendix). The SQUID magnetometer is particularly well suited to measure the AC susceptibility in the quasi-static limit ($\omega \to 0$). A frequency of 10 Hz allows good noise suppression at an acceptable measuring time. A second magnetometer (see Appendix), based on the mutual inductance technique, is used in combination with a lock-in amplifier (EG&G PARC Model

5302) to extend the AC susceptibility measurements up to frequencies of 1 MHz in the temperature range between 1.5 and 4.2 K (pumped ^{4}He cryostat). The linearity of the response to the applied AC field has been verified for AC field amplitudes from 0.1 to 500 μT. In all measurements the external magnetic fields (DC and AC) are carefully aligned parallel to the symmetry axis of the cylinders, so that above H_{c2} surface superconductivity can only nucleate on the cylindrical walls and not on the end faces. The demagnetization factor $N_Z = 0.36$ derived from the initial slope of the DC magnetization curve $M(H) = -H/(1 - N_Z)$ agrees with the theoretical expression $N_Z = 1 - 1/(1 + qa/b)$ [18]. Here $q = 4/3\pi + 2/3\pi \tanh(1.27b/a \ \ln(1 + a/b))$, where $h = 2b$ is the height and a the radius of the cylinder. The magnetization and susceptibility data presented in the next sections have been corrected using this demagnetization factor.

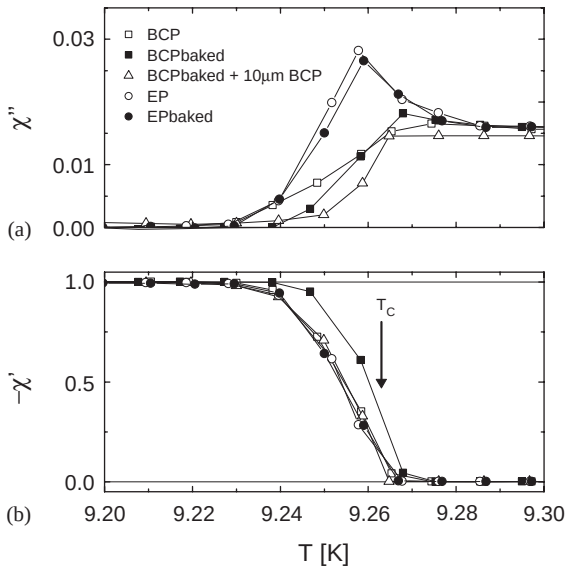

Fig. 1. (a) Imaginary and (b) real part of the linear AC susceptibility recorded near the zero-field transition temperature of the Nb-cylinders under investigation. Note the different χ''-scale in (a).

3. Bulk superconductivity

The superconducting transition temperature T_c is determined from the onset of the screening component χ' of the complex AC susceptibility $\chi = \chi' - i\chi''$, measured at vanishing DC field as a function of temperature (see Fig. 1). The average critical temperature $T_c = 9.263 \pm 0.003$ K of all samples agrees with the value $T_c = 9.25 \pm 0.01$ K reported by Finnemore et al. [19] for high purity Nb ($RRR = 1600 \pm 400$).

The complex AC susceptibility[1] $\chi(\omega) = \chi'(\omega) - i\chi''(\omega)$ is related to the conductivity of a cylinder of radius a by [20,21]

$$\chi'(\omega) - i\chi''(\omega) = \frac{2I_1(x)}{xI_0(x)} - 1$$
$$\text{with } x = \sqrt{i\omega a^2 \mu_0(\sigma'(\omega) - i\sigma''(\omega))}. \quad (3.1)$$

Here $I_0(x)$ and $I_1(x)$ are modified Bessel functions. For a short cylinder with height $h = 2a$ the radius must be replaced by $a/\sqrt{2}$.[2] The complex conductivity $\sigma(\omega)$ is obtained from the measured susceptibility $\chi(\omega)$ by means of an inversion routine [22]. The average Ohmic resistivity at 10 Hz and $T > T_c$ is found to be $\rho_n = (0.5 \pm 0.1)$ nΩ m, confirming the purity of the samples and the specification of the manufacturers of $RRR \simeq 300$. Very close to T_c the EP samples exhibit higher losses than the BCP ones. This is caused by a higher conductivity in a 100–500 μm surface layer.

In order to determine the thermodynamic critical field H_c the reversible magnetization $M_{rev} = (M_+ + M_-)/2$ is deduced from the hysteresis loops (Fig. 2), where M_+ corresponds to the ascending and M_- to the descending branch of the loop. The reversible magnetization of a BCP sample is plotted in Fig. 3a. The thermodynamic critical field is given by

$$H_c^2 = 2\mu_0 \int_0^{H_{c2}} M_{rev}(H)\,dH. \quad (3.2)$$

The critical field at $T = 0$ is derived using the empirical law

$$H_c(T) = H_c(0)(1 - (T/T_c)^2) \quad (3.3)$$

[1] The sign of the imaginary part refers to a time dependence $\exp(+i\omega t)$ of the electromagnetic fields.

[2] The effect of sample geometry on the relation between $\chi(\omega)$ and $\sigma(\omega)$ is extensively studied in Ref. [23].

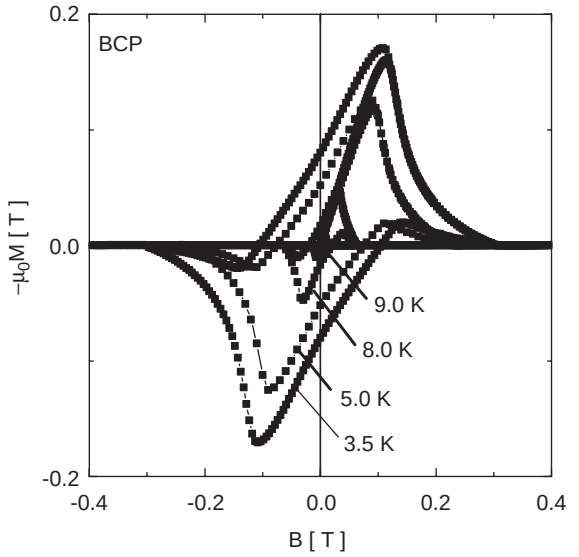

Fig. 2. Magnetization isothermal loops for a BCP sample. Plotted is $-\mu_0 M$ as function of the applied field $B = \mu_0 H$.

where T_c is given in Table 2. The upper critical field H_{c2} can be determined with high accuracy from the onset of the irreversible magnetization $M_{irr} = (M_+ - M_-)/2$, as shown in the inset of Fig. 3b. The H_{c2} data are well described by the temperature dependence [24]

$$H_{c2}(T) = H_{c2}(0)\frac{(1-(T/T_c)^2)}{(1+(T/T_c)^2)}. \quad (3.4)$$

The thermodynamic and upper critical fields[3] are plotted in Fig. 4 as functions of temperature. Averaged over all samples we get $B_{c2}(0) = \mu_0 H_{c2}(0) = 410 \pm 5\,\mathrm{mT}$ and $B_c(0) = \mu_0 H_c(0) = 180 \pm 5\,\mathrm{mT}$ (see also Table 2). While $B_{c2}(0)$ agrees with the upper critical field reported in Ref. [19] for pure niobium, our $B_c(0)$ is 10% smaller than the value $B_c(0) = 199 \pm 1$ mT quoted in Ref. [19].

Within the Ginzburg–Landau (GL) theory it is possible to determine the GL parameter at zero temperature $\kappa(0) = B_{c2}(0)/(\sqrt{2}B_c(0)) = 1.61 \pm 0.07$, the GL coherence length $\xi(0) = \sqrt{\hbar/(2eB_{c2}(0))} = 28.3 \pm 0.2\,\mathrm{nm}$ and the London penetration depth $\lambda_L(0) = \kappa(0)\xi(0) = 46 \pm 2\,\mathrm{nm}$.

[3]In this paper we use the SI unit system and quote magnetic fields in the form $B = \mu_0 H$ with the unit Tesla.

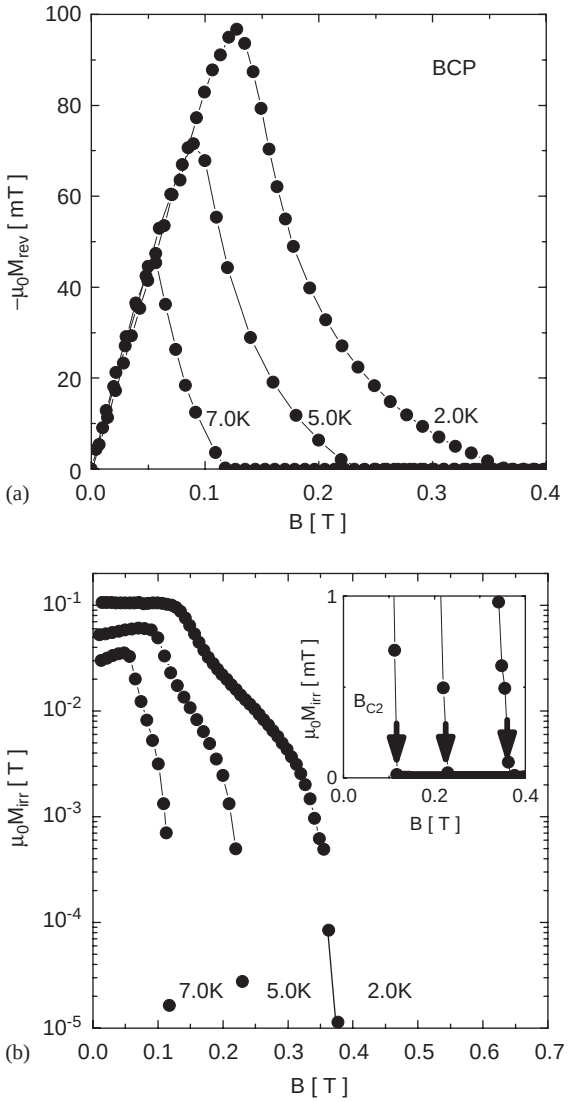

Fig. 3. (a) Reversible magnetization of a BCP sample at 2–7 K, evaluated from the isothermal loops. EP and/or baked samples show similar results. (b) Irreversible magnetization at 2, 5 and 7 K, showing the sharp onset of bulk superconductivity at $B_{c2}(T) = \mu_0 H_{c2}(T)$.

The data from differently treated samples are in good agreement and confirm the expectation that neither electropolishing nor low-temperature bakeout change the superconductor parameters of the bulk niobium.

The hysteresis loops observed in the magnetization measurements are a clear proof of magnetic

Table 2
Parameters of the Nb samples

	BCP	EP
T_c (K)	9.263 ± 0.003	
RRR	≈ 300	
Surf. roughness on grain (nm)	≈ 1	
Steps at grain bound	1–5 μm	$\lesssim 0.1$ μm
$B_c(0)$ (mT)	180 ± 5	
$B_{c2}(0)$ (mT)	410 ± 5	
$J_c(0,0)$(A/mm^2)	240 ± 10	180 ± 10

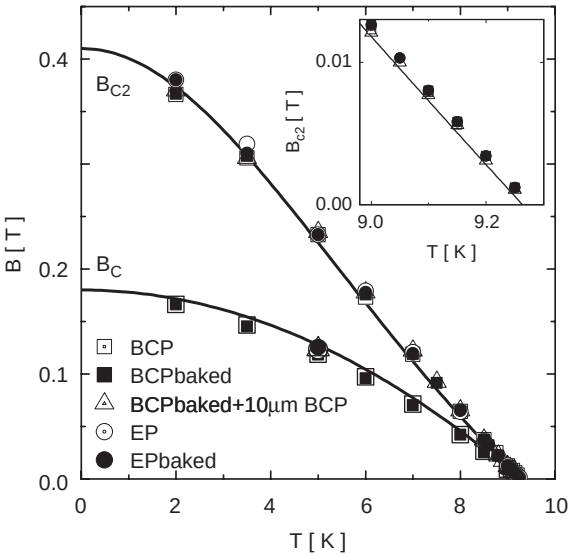

Fig. 4. Temperature variation of the upper critical field $B_{c2} = \mu_0 H_{c2}$ and of the thermodynamic critical field B_c of all cylinders. Solid curves: fits based on Eqs. (3.3) and (3.4). The expected linear behaviour of B_{c2} close to T_c is displayed in the inset.

flux pinning. Under the assumption that pinning in the bulk dominates one can derive the critical current density from the irreversible part of the magnetization: $J_c = 3M_{irr}/a$, where a is the radius of the Nb cylinder. We obtain $J_c = 240\,\mathrm{A/mm^2}$ for the BCP samples and $J_c = 180\,\mathrm{A/mm^2}$ for the EP samples (both at $T = 4.2\,\mathrm{K}$ and $B = 0$). Since EP does not affect the bulk this difference implies that surface flux pinning plays an important role too. Large variations of J_c between 10 and 1000 A/mm^2, depending on the mechanical and thermal treatment, were previously found by De Sorbo [25] and Das Gupta et al. [26] for Nb with $RRR \simeq 500$ respectively $RRR \simeq 40$.

4. Surface superconductivity

4.1. Critical surface field

Almost four decades ago Saint-James and de Gennes [27] discovered the nucleation of superconducting regions in a thin surface sheath in fields significantly higher than the critical magnetic field for nucleation in the volume, $B_{c3} = 2.392\kappa B_c$. For a type II superconductor as Nb the critical surface field is given by $B_{c3} = 1.695 B_{c2}$ [27]. Owing to the high sensitivity of the SQUID magnetometer, evidence for surface superconductivity in the field range $B_{c2} < B < B_{c3}$ is in fact observable in all samples. In Fig. 5 we show the complex AC susceptibility $\chi' - i\chi''$ at 5.0 K and 10 Hz as a function of the applied DC field for samples with different surface treatments: BCP, EP, baked and unbaked. The data at higher frequencies obtained with the mutual inductance magnetometer are presented in Section 5.3.

Approaching the transition to superconductivity from the normal state, i.e. from high fields, the nucleation field B_{c3} is commonly defined [28,29] by the onset of screening, i.e., the appearance of a finite $|\chi'|$ above the susceptibility value χ'_n in the normal state. We observe a strong dependence of B_{c3} on the surface condition: the BCP sample has the lowest B_{c3}, and both EP and baking increase the critical surface field.

The AC susceptibility of a BCP sample at temperatures between 3.5 and 9.0 K is plotted in Fig. 6. Similar measurements have been performed for all samples. The temperature dependence of B_{c3} for samples with different surface treatment is shown in Fig. 7. The data are well described by the relation

$$B_{c3}(T) = r_{32}\, B_{c2}(T) \tag{4.1}$$

where the ratio r_{32} depends on the surface preparation but not on the temperature, see Table 3 and Fig. 8.

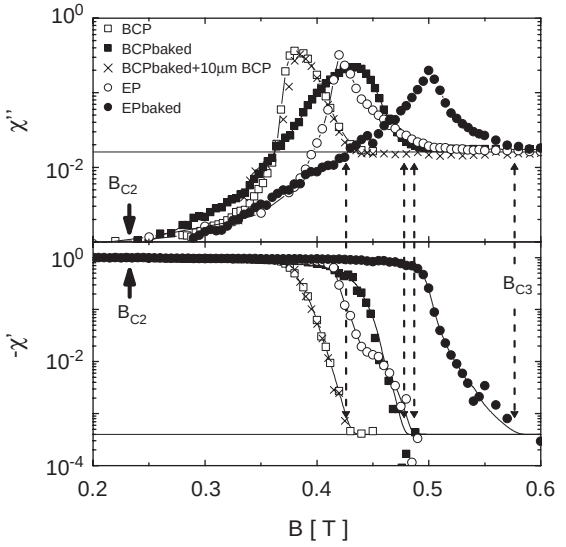

Fig. 5. Field dependence of the AC susceptibility on a logarithmic scale of Nb cylinders with different surface conditions. The data have been taken at $T = 5.0\,\mathrm{K}$, $f = 10\,\mathrm{Hz}$ and $B_{ac} = 1\,\mu\mathrm{T}$. The surface nucleation fields B_{c3} (arrows) are defined by the onset of an excess absorption ($\chi'' - \chi_n''$) or excess shielding ($\chi' - \chi_n'$), where χ_n'' resp. χ_n' are the imaginary resp. real part of χ in the normal state (indicated by the horizontal solid lines).

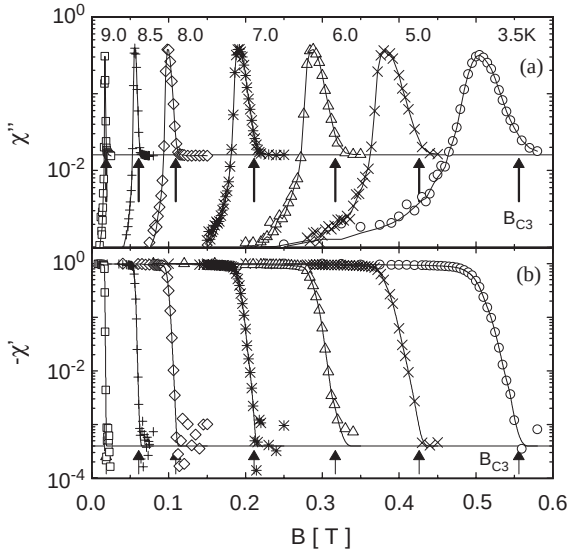

Fig. 6. (a) Imaginary and (b) real part of the AC susceptibility of a BCP-treated sample as a function of field for temperatures between 3.5 K and 9.0 K.

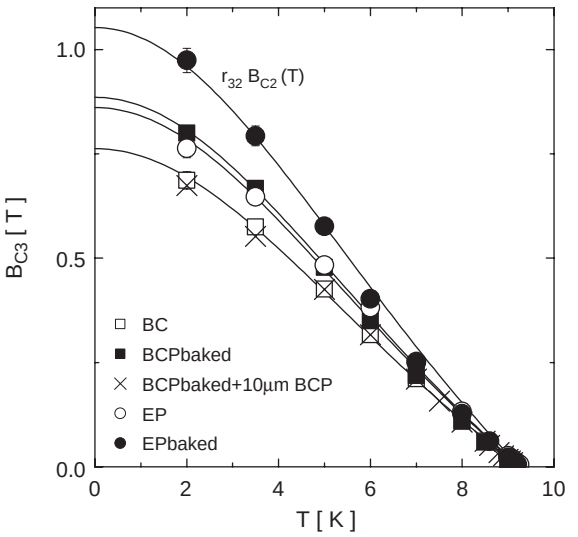

Fig. 7. Temperature dependence of critical surface field $B_{c3} = \mu_0 H_{c3}$ of the samples shown in Fig. 5. The data are fitted to the function $B_{c3}(T) = r_{32} B_{c2}(T)$, where the ratio r_{32} depends on the surface preparation but not on temperature. This means that B_{c2} and B_{c3} have the same temperature dependence.

The reproducibility of the measurements of the ratio r_{32} has been demonstrated on six BCP samples, two for each of the Nb producers (all Nb sheets have $RRR \approx 300$). The average value for the BCP samples is $r_{32} = 1.86 \pm 0.03$ and hence larger than the Ginzburg–Landau value $r_{GL} = 1.695$.

If a BCP sample receives an electropolishing of 80 μm the ratio r_{32} grows by ~12%. Also a low temperature baking (LTB) increases the ratio r_{32} considerably, see Fig. 8. Here the reproducibility has been demonstrated on six BCP samples, two for each of the Nb producers, which were baked for 48 h at 120 °C and yielded $r_{32} = 2.33 \pm 0.05$. In the bakeout at 123 °C the ratio r_{32} grows with increasing baking time. At 144 °C a saturation value of $r_{32} = 2.59 \pm 0.05$ is reached after 24 h without further increase towards longer baking times. The gain in the ratio r_{32} is completely lost if a 1 μm surface layer is removed by chemical etching. This proves that only a thin surface layer is modified by the bakeout.

Baking at 100 °C yields only a slight rise in r_{32}. Moreover, no appreciable change is observed by extending the baking time from 24 to 96 h. This

Table 3
The ratio $r_{32} = B_{c3}/B_{c2}$ for all samples

Sample	$r_{32} = B_{c3}/B_{c2}$
BCP only	1.86 ± 0.03
BCP + baking	
BCP + 24 h 100 °C	1.93 ± 0.05
BCP + 48 h 100 °C	1.93 ± 0.05
BCP + 96 h 100 °C	1.93 ± 0.05
BCP + 48 h 120 °C	2.16 ± 0.03
BCP + 24 h 123 °C	2.17 ± 0.05
BCP + 48 h 123 °C	2.33 ± 0.05
BCP + 96 h 123 °C	2.32 ± 0.05
BCP + 24 h 144 °C	2.59 ± 0.05
BCP + 48 h 144 °C	2.59 ± 0.05
BCP + 96 h 144 °C	2.59 ± 0.05
BCP + baking + BCP	
BCP + 48 h 120 °C + 1 μmBCP	1.90 ± 0.03
BCP + 48 h 120 °C + 5 μm BCP	1.87 ± 0.03
BCP + 48 h 120 °C + 10 μm BCP	1.86 ± 0.03
BCP + EP	
BCP + 40 μm EP	1.92 ± 0.05
BCP + 80 μm EP	2.10 ± 0.03
BCP + 145 μm EP	1.99 ± 0.05
BCP + 165 μm EP	1.99 ± 0.05
BCP + EP + baking	
BCP + 40 μm EP + 48 h 123 °C	2.64 ± 0.05
BCP + 80 μm EP + 48 h 123 °C	2.57 ± 0.05
BCP + 145 μm EP + 48 h 123 °C	2.40 ± 0.05
BCP + 165 μm EP + 48 h 123 °C	2.40 ± 0.05

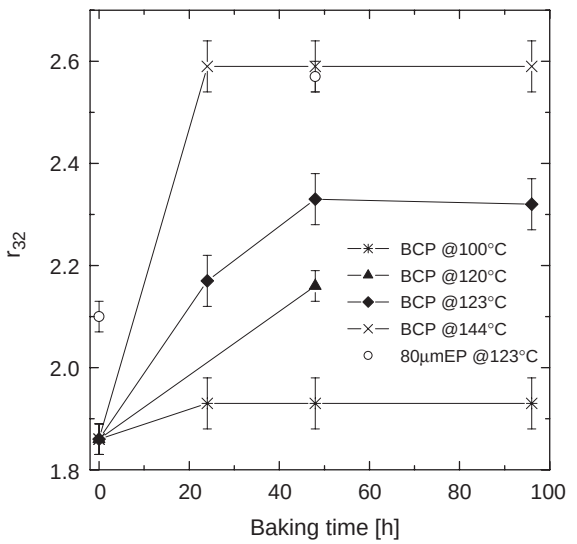

Fig. 8. The ratio $r_{32} = B_{c3}/B_{c2}$ as a function of baking time for BCP and EP samples at different baking temperatures.

means that 100 °C is probably too low a temperature for changing the superconductor properties at the Nb surface significantly.

The existence of a critical surface field exceeding the upper critical field of the bulk, $B_{c3} = r_{GL}\, B_{c2}$ with $r_{GL} = 1.695$, was predicted by Saint-James and de Gennes [27] by solving the linearized Ginzburg–Landau equation in the presence of a plane boundary which creates a mirror image of the potential. If we retain this idea the increased ratio $r_{32} > r_{GL}$ may be explained by assuming a larger value of B_{c2} close to the surface, $B_{c2}^{surf} > B_{c2}^{bulk}$, and by relating B_{c3} to this field: $B_{c3} = r_{GL}\, B_{c2}^{surf}$. The enhanced B_{c2}^{surf} may be caused for instance by a higher concentration of impurities and a reduced coherence length.

One obvious contaminant is oxygen. After the discovery of the bakeout effect in cavities systematic studies have been conducted on the morphological and chemical structure of niobium samples, for instance by surface-sensitive methods such as XPS (X-ray induced photoelectron spectroscopy) [30–32]. These studies indicate that baking causes a partial disintegration of the external Nb_2O_5 layer, the formation of suboxides (NbO, NbO_2) and most likely oxygen dissolution.

The effect of interstitial oxygen on the upper critical field of niobium was studied by Koch et al. [33]. The concentration c_O of oxygen in atomic per cent can be derived from an expression valid at 4.2 K [26]

$$c_O[\text{at\%}] = 1.475 \times 10^{-3}(B_{c2}^{surf}[\text{mT}] - 276).$$

Under the assumption that the enhanced surface fields B_{c2}^{surf} are indeed caused by oxygen this formula is used to compute the oxygen concentration listed in Table 4. Fig. 9 shows that the oxygen concentration increases if a BCP sample is subjected to EP or LTB.

In a study on BCP cavities recently performed at Jefferson Lab, Ciovati et al. [14] measured an average surface $RRR = 206 \pm 3$. Under the same assumption that oxygen is the main contaminant they find $c_O = 0.017$at% which, considering the different BCP conditions in the two laboratories, is in reasonable agreement with our results for BCP samples of $c_O = 0.035$at%.

Table 4
Parameters of the oxygen-contamination model and the Shmidt model

Sample	c_O (at%O)	d_{min} (nm)	ℓ_{max} (nm)
BCP only	0.035	2.5	436
BCP + baking			
24 h 100 °C	0.052	3.5	318
48 h 100 °C	0.052	3.5	318
96 h 100 °C	0.052	3.5	318
48 h 120 °C	0.106	6.5	169
24 h 123 °C	0.109	6.5	166
48 h 123 °C	0.147	8.5	125
96 h 123 °C	0.144	8.5	127
24 h 144 °C	0.209	12	90
48 h 144 °C	0.209	12	90
96 h 144 °C	0.209	12	90
BCP + baking (48 h at 120 °C) + short BCP			
1 μm BCP	0.045	3	360
5 μm BCP	0.037	2.5	414
10 μm BCP	0.035	2.5	436
BCP + EP			
40 μmEP	0.049	3	331
80 μm EP	0.092	6	192
145 μm EP	0.066	4	259
165 μm EP	0.066	4	259
BCP + EP + baking (48 h at 123 °C)			
40 μm EP	0.221	13	85
80 μm EP	0.204	12	92
145 μm EP	0.163	9.5	113
165 μm EP	0.163	9.5	113

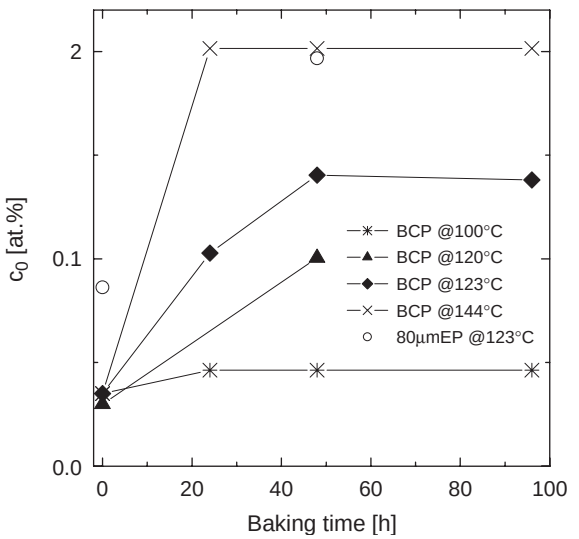

Fig. 9. Oxygen concentration as a function of baking time for different surface treatments.

Shmidt [34] has proposed a model in which the impurities are contained in a layer whose thickness is less than the coherence length of the bulk $d \leqslant \xi$. This model predicts the following relation:

$$r_{32} = 1.67\left(1 + (1-\chi_G)\sqrt{1.7}\frac{d}{\xi(T)}\right). \tag{4.2}$$

Here χ_G is the Gor'kov impurity function which relates the GL κ parameters in the pure bulk and the point defected surface, $\chi_G = \kappa/\kappa_{surf}$. Since $(1-\chi_G) \leqslant 1$ and $d/\xi \leqslant 1$ the maximum ratio is $r_{max} \leqslant 3.8$, which is consistent with our results. Eq. (4.2) embodies two unknowns, the mean free path ℓ and the thickness d along with $\xi_0 = 1.35\,\xi(0)$ [35], hence we can only consider limiting cases. In the dirty limit $\ell \to 0$ ones gets $\chi_G \simeq 1.33\,\ell/\xi_0 \to 0$ and r_{32} increases with increasing thickness d of the contaminated layer. The minimum values of d in the dirty limit are listed in Table 4. In the clean limit $\ell \gg \xi_0$ one has $\chi_G \simeq 1 - 0.884\,\xi_0/\ell$, hence the maximum value of ℓ is given by putting $d = \xi$. The results are listed in Table 4. Both the oxygen contamination model and the Shmidt model are consistent with the idea of oxygen diffusion during baking from the ~5 nm thin Nb_2O_5 sheath into deeper layers [11].

5. Coherent surface superconductivity

5.1. Surface conductivity and resistivity

We now examine in more detail the behaviour of the niobium samples for applied magnetic DC fields in the range between B_{c2} and B_{c3} where only a thin surface sheath is superconducting while the bulk is in the normal state. Coming down from high fields, the screening part of χ starts to grow upon crossing B_{c3}. Owing to the high sensitivity of the SQUID magnetometer, the onset of screening is clearly visible when $-\chi'$ is plotted on a logarithmic scale (Fig. 10). This allows a precise determination of the critical surface field B_{c3}. On a linear scale, however, the onset of surface superconductivity is barely visible, while a strong rise of $-\chi'$ is observed at a lower field B_{c3}^{coh}. Following Ref. [36], we call this field the *coherent*

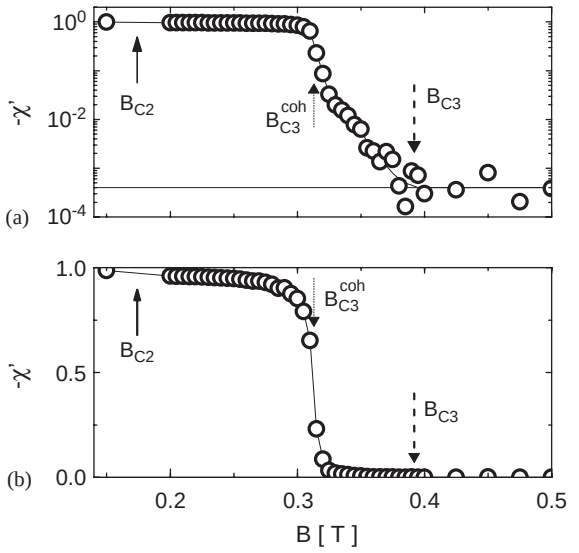

Fig. 10. The negative real part of the susceptibility of an EP cylinder at 6.0 K and 10 Hz as a function of the applied field. (a) Plotted as in Fig. 5 on a logarithmic scale. The start of the growth of $|\chi'|$ defines the critical surface field $B_{c3} = \mu_0 H_{c3}$. (b) The same data on a linear scale. The field B_{c3}^{coh} marks the onset of coherent surface superconductivity with a strong growth of $|\chi'|$ towards $|\chi'| = 1$.

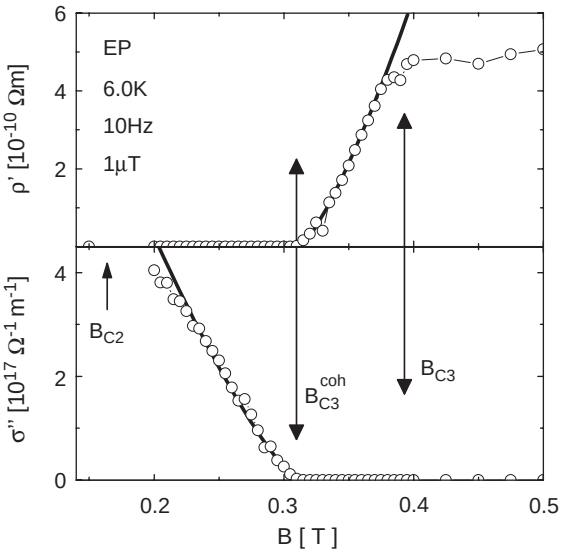

Fig. 11. Top: the real part of the resistivity ρ' of an EP sample as a function of field. For $B > B_{c3}^{coh}$ the data are well described by the power law curve $\rho' \propto |B - B_{c3}^{coh}|^{1.3}$. Bottom: the imaginary part of the conductivity in comparison with the power law $\sigma'' \propto |B_{c3}^{coh} - B|^{1.3}$.

critical surface field, for reasons explained below. It is still well above the nucleation field B_{c2} of the bulk.

To gain a deeper insight into the physical mechanisms in this region it is instructive to study the field dependence of the complex conductivity $\sigma = \sigma' - i\sigma''$ and the resistivity $\rho = 1/\sigma = \rho' + i\rho''$. These quantities can be calculated from the AC susceptibility with the help of Eq. (3.1). As can be seen from Fig. 11, in the range $B_{c3} > B > B_{c3}^{coh}$ the resistivity ρ' is sharply dropping with decreasing B, while there is only very little screening, $\sigma'' \simeq 10^{10}\Omega^{-1}\,\mathrm{m}^{-1}$ at 10 Hz. This can be interpreted in the following way: for applied fields $B_{c3} > B > B_{c3}^{coh}$ the surface sheath is not uniformly superconducting but only in disconnected domains such that super-currents flowing around the entire Nb cylinder are impeded. The situation changes dramatically when the applied field falls below B_{c3}^{coh}: here the Ohmic resistivity ρ' vanishes and the imaginary part σ'' of the conductivity rises steeply with decreasing field. Since $\omega\sigma''$ is proportional to the Cooper pair density,[4] it was proposed in Ref. [36] to associate B_{c3}^{coh} with the onset of long-range superconductivity in the surface sheath. This observation justifies the name coherent surface field. Slightly below B_{c3}^{coh} the susceptibility reaches the value $\chi' = -1$ which is characteristic of complete shielding.

The singular behaviour of ρ' and σ'' near the transition to coherent surface superconductivity can be described by power laws in $|B - B_{c3}^{coh}|$, see Fig. 11. Above the transition one gets

$$\rho'(B) \propto (B - B_{c3}^{coh})^s \quad \text{for } B_{c3}^{coh} < B < B_{c3} \tag{5.1}$$

while below the transition

$$\sigma''(B) \propto (B_{c3}^{coh} - B)^t \quad \text{for } B_{c2} < B < B_{c3}^{coh}. \tag{5.2}$$

For the EP samples (baked and unbaked) the exponents are found to be equal: $s = t = 1.3 \pm 0.1$,

[4] In the two-fluid model of superconductivity, the imaginary part of the AC conductivity is given by $\sigma'' = 2n_c e^2/(m_e\omega)$ where n_c is the Cooper pair density, see for example Ref. [37].

see Figs. 11 and 12. This is consistent with a 2-D model of a percolation-driven transition to coherent superconductivity [36,38,39]. For the BCP samples, however, the exponents $s = 1.05 \pm 0.10$ and $t = 1.4 \pm 0.1$ are different (see Fig. 13), indicating a dimensionality of the percolating network which is slightly higher than two but still much smaller than three [40]. The power law analysis points to different surface topologies and electronic structures of BCP and EP samples. As expected, baking has no influence on the topology, and hence does not modify the exponents.

An interesting observation is that the coherent critical surface field is always a fixed fraction of the

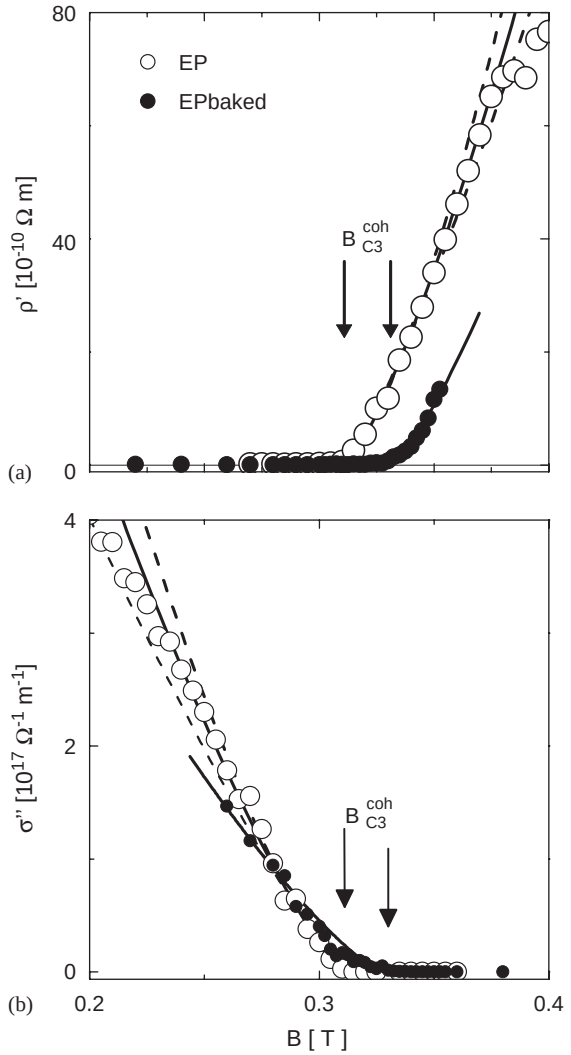

Fig. 12. Analysis of the singular behaviour (a) of the real part of the resistivity ρ' and (b) of the imaginary part of the conductivity σ'' of an electropolished Nb cylinder at 6 K. Open circles: before baking, closed circles: after baking. The solid curves are power-law fits revealing the same exponents before and after baking. Note that the coherent surface field is larger after baking.

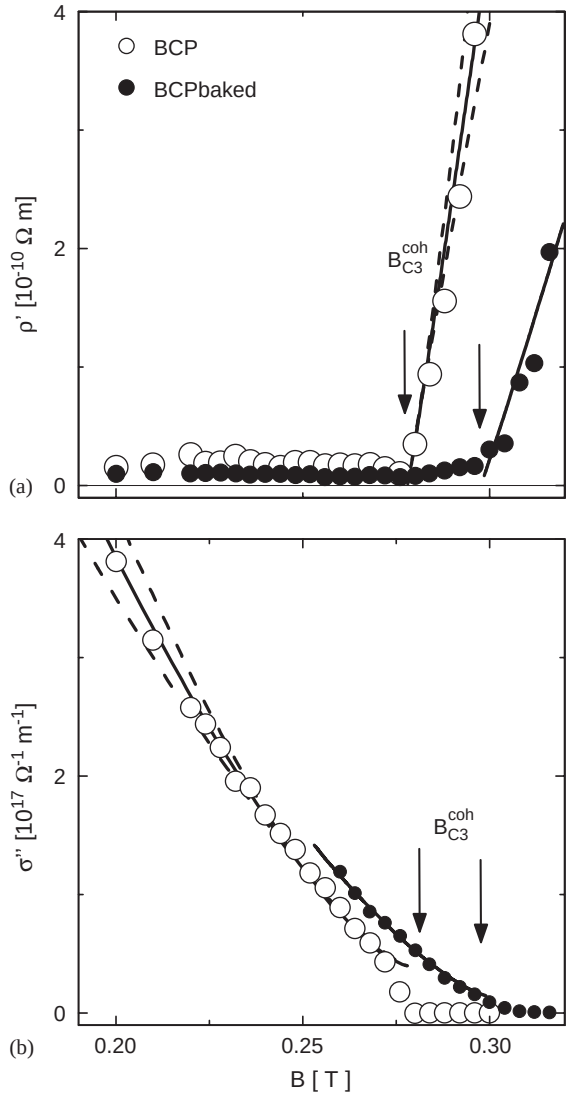

Fig. 13. (a) The real part of the resistivity ρ' and (b) the imaginary part of the conductivity σ'' of a chemically etched (BCP) cylinder. Open circles: before baking, closed circles: after baking. Test temperature 6 K.

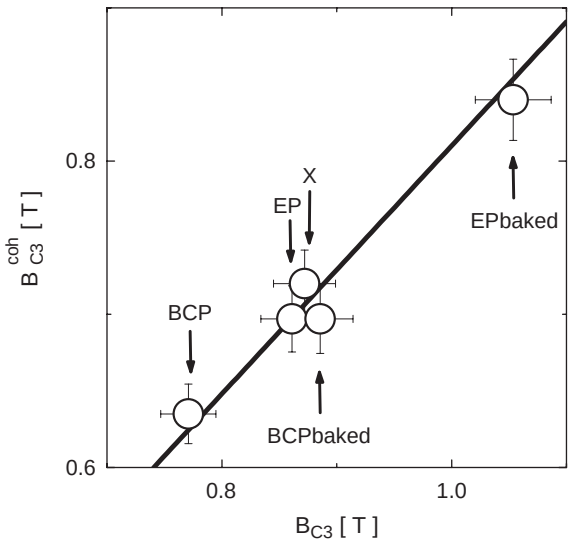

Fig. 14. Linear relation between B_{c3}^{coh} and B_{c3} obtained for samples with different surface treatment. The data point labelled "X" refers to an Nb single crystal with an etched surface [38].

Ginzburg–Landau type surface field: $B_{c3}^{coh} = (0.81 \pm 0.02)B_{c3}$, independent of the surface topology, see Fig. 14. This suggests some intrinsic but yet unknown effect behind the formation of the coherent surface superconductivity.

5.2. Frequency dependence of the conductivity

Up to now we have discussed the AC susceptibility and conductivity in the quasi-static limit at $f = 10$ Hz. The investigations have been extended up to 1 MHz. In Fig. 15, the quantity $\omega\sigma''$, which is a measure of the superfluid density, and the loss component σ' are shown as functions of the applied field for frequencies between 10 Hz and 1 MHz. In the normal conducting regime above B_{c3} we find that $\sigma' = \sigma_n = (2.1 \pm 0.3)10^9(\Omega\text{m})^{-1}$ is frequency independent and also field independent since it agrees with the value obtained in zero field (see Section 2). Below B_{c3}, σ' becomes frequency dependent.

From the field dependence of $\omega\sigma''$ it is possible to distinguish five phases of the samples obtained by sweeping the DC magnetic field [39]. The indicated critical fields separate the Meissner phase

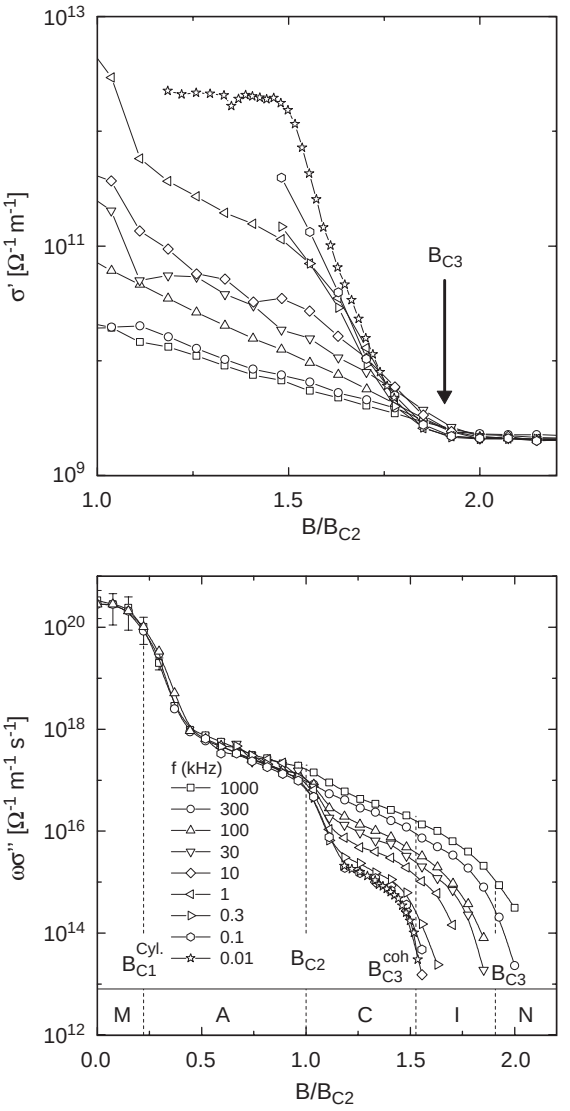

Fig. 15. The complex conductivity $\sigma(\omega)$ as a function of field for frequencies between 10 Hz and 1 MHz. The top graph shows σ', the bottom graph $\omega\sigma''$. The indicated critical fields B_{c1}, B_{c2}, B_{c3}^{coh} and B_{c3} separate five phases: Meissner M, Abrikosov A, coherent surface superconductivity C, incoherent surface superconductivity I, normal state N.

(M), the Abrikosov vortex lattice phase (A), the coherent surface phase (C), the incoherent surface phase (I), and finally the normal phase (N). The two surface phases are depicted schematically in Fig. 16. The Meissner and Abrikosov phase are

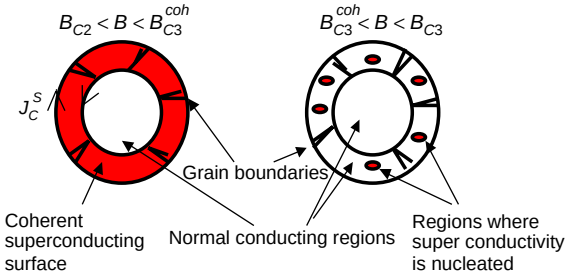

Fig. 16. Schematic view of the coherent and incoherent surface phases of a superconducting cylinder.

frequency independent. The strongest frequency variation is observed close to the coherent surface field B_{c3}^{coh}. The frequency dependence close to B_{c3}^{coh} can be used to check the validity of dynamical scaling, see Ref. [36].

5.3. Surface critical currents

As a further evidence for the coherence of the surface superconductivity below B_{c3}^{coh}, a finite critical current has been detected [36,38,39]. To this end, a small longitudinal gradient in the DC magnetic field B of the SQUID magnetometer has been utilized, the field inhomogeneity being 0.0025%/mm. During the motion of the sample through the pickup coil with a velocity v_z the field gradient induces an azimuthal electric field along the circumference of the cylinder of radius a

$$E_\phi = -\frac{av_z}{2}\frac{dB}{dz}.$$

Depending on the direction of motion, the response is either diamagnetic or paramagnetic. These responses are symmetric with respect to the linear background $M_{el}(H) = \chi_{el} B/\mu_0$ due to the paramagnetism of the normal conduction electrons in niobium (see Section 6). The induced surface current per unit length

$$J_c^s(B) = M - \chi_{el} B/\mu_0 \tag{5.3}$$

is shown in Fig. 17 for all samples as a function of the reduced field $(B_{c3}^{coh} - B)/(B_{c3}^{coh} - B_{c2})$ at 2.0 K. An important observation is that $J_c^s(B)$ does not depend on the scan velocity v_z, which has been varied between 0.1 and 40 mm/s (see Fig. 18). This

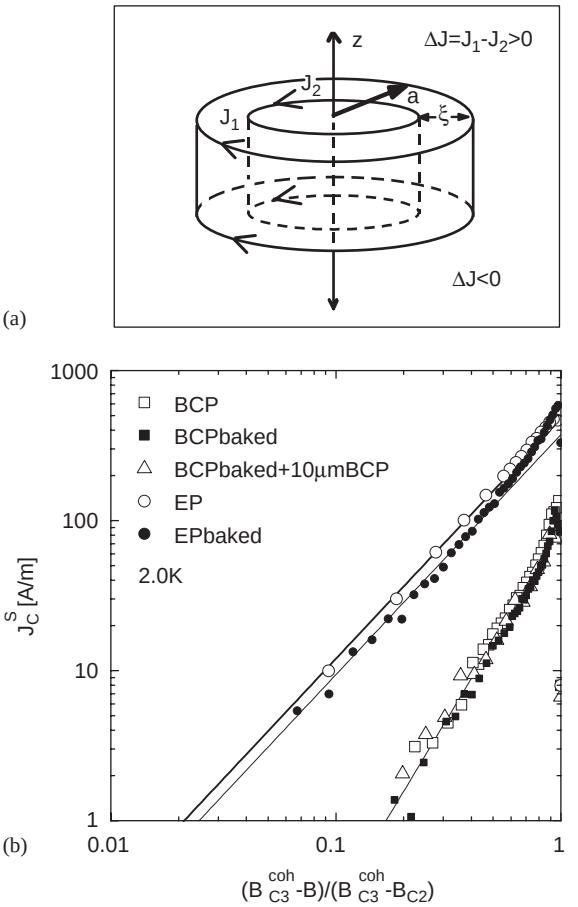

Fig. 17. (a) Schematics of the surface supercurrents according to Fink and Barnes [42]. (b) Dependence of the surface current per unit length J_c^s on the normalized magnetic field $(B_{c3}^{coh} - B)/(B_{c3}^{coh} - B_{c2})$ for all samples ($T = 2$ K).

indicates that E_ϕ is always large enough to excite the critical surface supercurrent density in the cylinder, $J_c^s(B)$.

According to Abrikosov [41] the surface current density (current per unit length) should obey a power law

$$J_c^s(B) \propto \left(1 - \frac{B}{B_{c3}}\right)^v \tag{5.4}$$

with $v = 1.5$. For the EP samples we find an exponent $v = 1.6 \pm 0.1$, consistent with the Abrikosov calculation. The measured currents per unit length of 477 ± 24 A/m (unbaked) and 374 ± 24 A/m (baked) are in good agreement with predictions

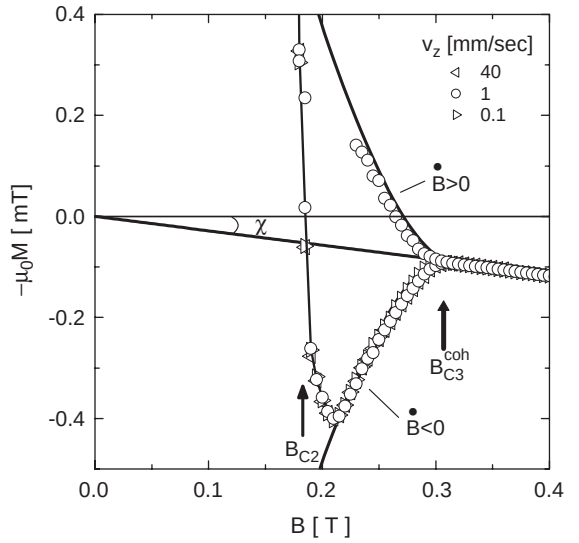

Fig. 18. Magnetization of an EP cylinder between B_{c2} and B_{c3}^{coh} at 6 K measured along positive and negative field gradients. Above B_{c2}, the magnetization is independent of the scan velocity v_z. Note the small values of the magnetization.

by Fink and Barnes [42] who consider a multiply connected surface sheath with two currents flowing in the opposite direction as illustrated by Fig. 17a. In this sense, our surface current (5.3) must be interpreted as the difference between two large counter-rotating currents. We observe a clear difference between electropolished and chemically etched samples: the BCP cylinders have a factor of six smaller critical surface currents and the exponent is larger, $v = 2.5 \pm 0.3$.

Following Ref. [36] we compare the exponent v with the scaling prediction for a multidimensional percolation network, $v = t - \Delta$ [43]. For the EP sample the magnitude of the so called *twistedness index* of the macrobond, $\Delta = t - v = -0.3 \pm 0.3$ is in agreement with the small and negative value found for 2-D granular superconducting PbGe films [43]. The higher value of Δ for the BCP samples indicates that the surface currents have to follow more complicated orbits than in EP samples. The lower surface current densities J_c^s in BCP-treated surfaces and the higher twistedness index Δ are possibly related to the larger roughness at the grain boundaries.

The surface currents per unit length, as measured in our experiment, are three orders of magnitude lower than the currents that would be needed to excite a niobium cavity to RF magnetic fields beyond $H_{c2} \approx 3 \times 10^5$ A/m. However, our quasi-static measurements ($f = 10$ Hz) do not exclude the possibility that much higher surface currents might exist in the non-equilibrium state of superconductivity which is relevant for high-frequency cavities.

6. Paramagnetic susceptibility

By measuring the magnetic susceptibility in a large external field $B = 0.7$ T where the entire sample is in the normal state it is possible to search for magnetic impurities in the niobium. The data are shown in Fig. 19a for temperatures between 2 and 300 K. Above 50 K our results on the paramagnetic susceptibility χ_{el} of the normal conduction electrons in Nb are in excellent agreement with previous measurements by Hechtfischer [44]. Below 50 K an additional contribution to χ is observed, which obeys a Curie–Weiss law

$$\chi - \chi_{el} = C/(T - \theta),$$

see Fig. 19b. The fit values for the Curie constant C and the Curie–Weiss temperature θ are listed in Table 5. Such behaviour indicates the presence of localized magnetic impurities. While $\theta \simeq -1$ K for all samples, the Curie constant, being proportional to the concentration of the localized magnetic moments, increases during the bakeout.

Oxygen vacancies in the Nb_2O_5 sheath would be a good candidate for localized magnetic moments [45]. Their Curie–Weiss behaviour has been observed in $Nb_2O_{5-\delta}$ crystallographic shear structures with $C \simeq 10$ mK for $\delta \approx 0.17$ [45]. Assuming the shear structure to be present in the $d \simeq 5$ nm thin Nb_2O_5 layer, one expects a Curie constant $C = 3d/a \times 10$ mK ≈ 0.12 μK. Since this is more than two orders of magnitude smaller than the values in Table 5, oxygen vacancies in the Nb_2O_5 sheath cannot account for the observed magnetic behaviour.

The paramagnetism of other impurities, which may be introduced by the BCP and EP processes,

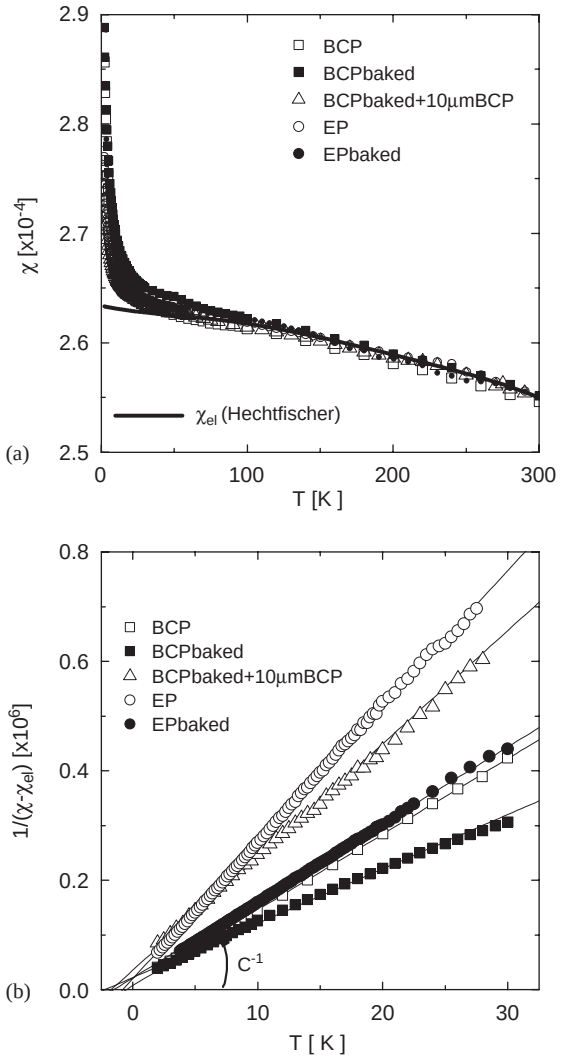

Fig. 19. (a) Temperature dependence of the susceptibility of all samples measured at $B = 700$ mT. (b) Curie–Weiss contribution to the paramagnetic susceptibility. Solid lines are fits to the Curie–Weiss law $(\chi - \chi_{el})^{-1} = (T - \theta)/C$.

Table 5
Curie constant C and Curie–Weiss temperature θ

Sample	C (μK)	θ (K)
BCP	72.3 ± 0.1	-0.5 ± 0.2
BCP baked	100.6 ± 0.07	-2.2 ± 0.1
EP	40.2 ± 0.3	-0.8 ± 0.2
EP baked	71.0 ± 0.1	-1.5 ± 0.2
BCP baked + 10 μm BCP	48.3 ± 0.4	-1.7 ± 0.3

like N, C, F, P, S, the hydrogen bonded H_2O/C_xH_y $(OH)_z$ [46] and some niobium suboxides NbO_x ($x \lesssim 1$), has not yet been investigated. Perhaps they form clusters with large paramagnetic moments. After baking, the Curie constant C is found to be increased by about 40–50%. One possibility would be that during baking additional magnetic moments are released from external or internal surfaces.

The observation that a BCP-treated sample has a significantly larger Curie constant than an EP sample indicates that the magnetic moments are not confined to the surface only but reside also deeper in the material, probably in the grain boundaries which are more pronounced in BCP than in EP surfaces.

7. Summary and conclusions

As expected, the bulk properties of the niobium samples, T_c, B_c, RRR and B_{c2}, remain invariant when different surface treatments such as chemical etching and electropolishing or a low-temperature bakeout are applied. In contrast to this, the superconducting properties of the surface itself are found to be strongly modified by these treatments. Evidence for surface superconductivity at fields exceeding the upper critical field B_{c2} of the bulk is found in all samples. The critical surface field B_{c3} is always larger than the value $B_{c3} = 1.695B_{c2}$ derived from the Ginzburg–Landau theory, the ratio $r_{32} = B_{c3}/B_{c3}$ amounts to 1.86 for BCP samples and 2.1 for EP samples. It increases further by baking the sample at 120–140 °C for 24–96 h. We interpret this enhanced surface field as being due to increased impurity contents of the niobium in a layer close to the surface and, related to this, a reduced electron mean free path. The upper values of the mean free path ℓ_{max} found by using the Shmidt model (see Table 4) are consistent with the measurements performed on BCP and BCP baked cavities by Ciovati et al. [14]. Our results are also consistent with the surface analysis studies performed on Nb [30–32] indicating that baking causes a partial disintegration of the external Nb_2O_5 layer, the formation of suboxides (NbO, NbO_2) and most

likely oxygen dissolution, causing a reduction in the mean free path. As observed in Fig. 9 the oxygen concentration at the surface c_O grows faster by raising the baking temperature than by increasing the baking time, which is expected for a diffusion process.

A most remarkable observation is that two different phases of surface superconductivity exist which are separated by a "coherent" critical surface field B_{c3}^{coh}: a coherent phase C for applied fields between B_{c2} and B_{c3}^{coh} with bipolar shielding currents going around the whole cylindrical sample, and an incoherent phase I between B_{c3}^{coh} and B_{c3} which is characterized by disconnected superconducting regions with normal zones in between. Both B_{c3}^{coh} and B_{c3} depend on the surface preparation but the ratio B_{c3}^{coh}/B_{c3} has the value 0.81 for all samples: BCP, EP, unbaked and baked. A power-law analysis of the complex conductivity and resistivity reveals that at B_{c3}^{coh} a phase transition takes place between coherent and incoherent surface superconductivity. For the EP samples the exponents are in agreement with the expectation for percolation through a two-dimensional network of superconducting and resistive sections. A different behaviour is seen in the BCP samples, here the dimensionality of the network would have to be slightly larger than two. We suspect that this may be related to weak links at the grain boundaries and to more complicated, nonplanar current paths in the surface layer.

In the coherent phase C, a small net current around the Nb cylinder can be induced by a time-varying magnetic field whose direction depends on the sign of $\dot{B}$ according to Lenz's rule. However, this net current, being the difference of two counter-rotating currents, is only a few 100 A/m and thereby three orders lower than the RF currents that would be needed to operate an accelerating cavity at RF magnetic fields above $H_{c2} \approx 3 \times 10^5$ A/m. Our steady-state results do not exclude the possibility that higher surface currents might exist in non-equilibrium states, for instance in the high-frequency fields applied to accelerator cavities. In the BCP samples the surface currents are a factor of six lower which again points to weak links at grain boundaries.

An important result of our investigations is that the various surface preparation steps improving cavity performance have all a well-measurable influence on the magnetic properties of the samples. The critical surface field of a chemically etched (BCP) sample exceeds the theoretical value of $B_{c3} = 1.695 B_{c2}$ by about 10%. The electrolytic polishing process leads to an additional increase of 10%. The low temperature bakeout enhances B_{c3} even further by roughly 15% for BCP and 25% for EP samples. At $T = 2$ K the following numbers are found: $B_{c3} = 687 \pm 20$ mT for a BCP sample before baking and 800 ± 25 mT after baking; $B_{c3} = 764 \pm 25$ mT for an EP sample before baking and 974 ± 30 mT after baking. The critical exponents of the power law fits near B_{c3}^{coh} are different for EP- and BCP-treated samples: we get $s = t = 1.3 \pm 0.1$ for EP and $s = 1.05 \pm 0.1$, $t = 1.4 \pm 0.1$ for BCP samples. From this one can conclude that the smooth EP surface is able to support planar (two-dimensional) surface currents while the rough grain boundaries in a BCP surface enforce more complicated current patterns. The EP samples feature a coherent surface phase which resembles the Meissner phase in the bulk. In the BCP samples this coherent phase is disturbed by weak links at the grain boundaries.

The paramagnetic susceptibility in the normal-conducting regime is dominated by the normal conduction electrons in niobium but at low temperatures an additional contribution is observed which obeys a Curie–Weiss law and can be attributed to paramagnetic impurities. Their number is increased by low-temperature baking (LTB). This is in qualitative accordance with the generally accepted interpretation that LTB leads to a partial reduction of the Nb_2O_5 layer and an oxygen diffusion into deeper layers. Remarkably, the density of paramagnetic impurities is larger in BCP than in EP samples, which may be an indication that the impurities in grain boundaries play an important role.

In our view, the above observations are of high relevance for RF cavities and underline the superiority of electropolished surfaces. It must be emphasized, however, that measurements on niobium samples do not render cavity tests superfluous. One essential difference is that the samples

are investigated in a large DC background magnetic field with a superimposed small AC field while in the cavities the RF magnetic field assumes large amplitudes. It is by no means obvious that the superconductor responds in the same way to these different conditions. In particular, the dramatic improvement in the high-field performance of EP cavities by applying the low-temperature bakeout could certainly not have been predicted from the 20% growth of B_{c3} observed in EP-treated Nb samples. According to our understanding the underlying mechanisms of the bakeout effect are not yet fully understood.

Acknowledgements

Thanks are due to R. Anton (University of Hamburg) for his advice and the possibility to use his equipment for sample preparation, to N. Steinhau-Kühl (DESY) for carrying out the BCP and EP treatments of the samples, to D. Görlitz (University of Hamburg) for his help and to W. Gil (University of Hamburg) for SEM and AFM measurements on the samples. The work of S.C. was supported by the Deutsche Forschungsgemeinschaft through Grant No. CA 284/1-1.

Appendix A

The SQUID-Magnetometer $MPMS_2$ made by Quantum Design is an excellent apparatus to measure the DC magnetization and the AC susceptibility of samples with a very high sensitivity and over a wide range of magnetic fields and temperatures. A superconducting solenoid produces a DC field up to ± 1 T, and a copper coil with 8 turns produces AC-fields from 10 nT up to 0.5 mT, with frequencies from 0.01 Hz up to 1 kHz. The temperature can be varied from 2 K up to 350 K. The measurable range of magnetic moments extends up to $\pm 0.3\,\mathrm{Am}^2$ with a sensitivity of $10^{-10}\,\mathrm{Am}^2$.

The detection coil system is built as a gradiometer of second order and made from a single length of superconducting wire. The center coil with two turns is wound clockwise, the upper and lower coils are 14 mm away from the center coil and consists of a single turn each wound counterclockwise (see Fig. 20). This configuration cancels noise due to fluctuations in the large magnetic field of the superconducting magnet. Together with a transformer which couples the current changes to the RF-SQUID the pick-up-coil forms a closed superconducting loop.

For DC magnetization measurements, the sample is moved through the pickup coil at constant speed. The scan length is typically 40 mm, measurements are taken at 30–50 positions. At each position the motion is shortly stopped for the measurement. The current induced in the pickup coil by the moving sample is proportional to the magnetic moment of the sample.

The AC susceptibility is measured at two different positions: in the center coil of the pickup system and in the lower compensation coil. Before applying the AC field a nulling procedure is carried out to remove the induced signal from switching on the superconducting coil.

In the second magnetometer, sketched in Fig. 21, the measuring coil system consists of two identical coils wound in opposite direction. Without sample the induced voltage is almost balanced to zero. The sample is positioned in one of the two pickup coils so that the measured voltage is given by the following relation:

$$U = iI_{\mathrm{ac}}\omega M q_{\mathrm{f}}\chi \tag{A.1}$$

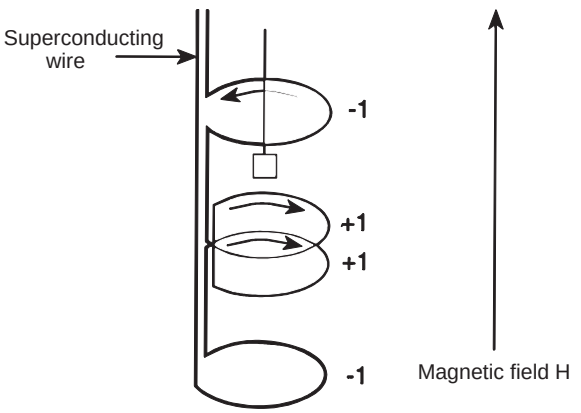

Fig. 20. Schematic coil configuration of the SQUID magnetometer.

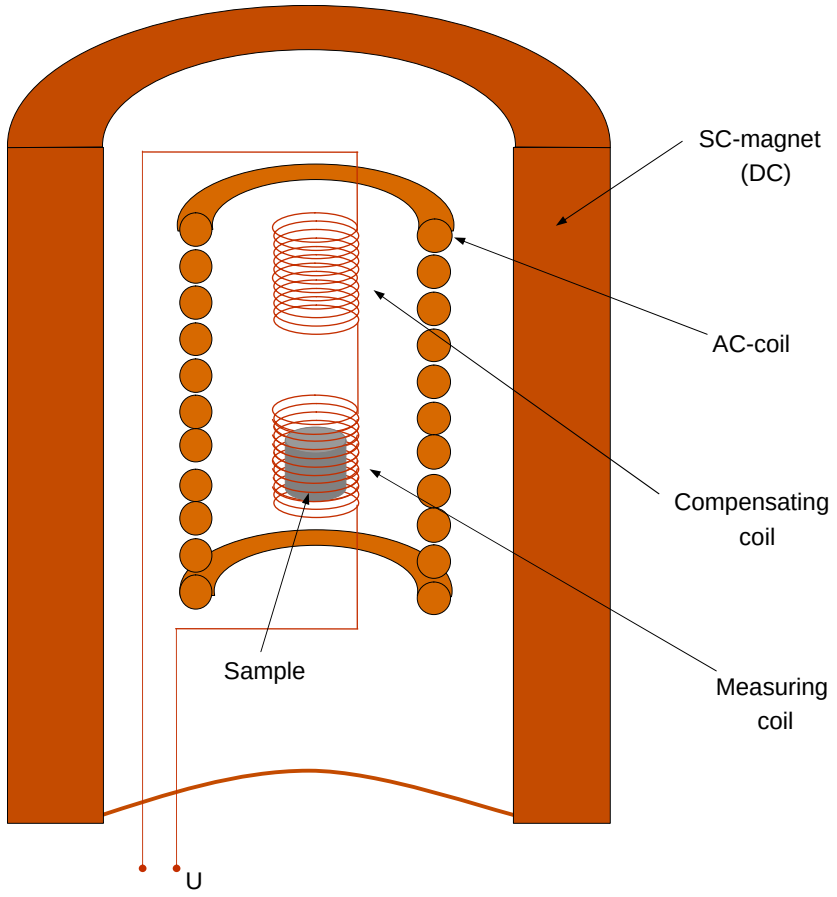

Fig. 21. Coil configuration of the mutual inductance magnetometer.

where $I_{ac} = I_0 \exp(i\omega t)$ is the current in the AC coil, M the mutual inductance coefficient between the AC coil and one of the pickup coils, q_f the filling factor given by the ratio of sample volume to coil volume and χ the AC susceptibility of the sample. Since the two pickup coils are not exactly identical there will be a background voltage U_b, that depends on the frequency and amplitude of the applied AC field.

$$U' = \cos\phi\,(U'_m - U'_b) + \sin\phi\,(U''_m - U''_b),$$
$$U'' = -\sin\phi\,(U'_m - U'_b) + \cos\phi\,(U''_m - U''_b)$$

where U'_m and U''_m are the real and imaginary part of the measured signal. The system is calibrated with a spherical $GdCl_3 \cdot 6H_2O$ sample of 3 mm diameter. For each AC amplitude and frequency the phase ϕ and the mutual coupling M are determined from the conditions $\chi'' = 0$ and $\chi' = C/T$, where $C = 0.65 \pm 0.01$ K is the known Curie constant of $GdCl_3 \cdot 6H_2O$.

References

[1] Gmelin, Handbuch der anorganischen Chemie, Vol. 49(Nb), Springer, Berlin, 1970.
[2] P. Kneisel, Surface preparations of niobium, in: M. Kuntze (Ed.), Proceedings of the Workshop on RF Superconductivity, Vol. I+II, KFK, Karlsruhe, 1980, p. 27, KFK-3019.
[3] B. Aune, et al., The Superconducting TESLA Cavities, Phys. Rev. STAB 3, 092001 (2000).
[4] K. Saito, et al., Superiority of electropolishing over chemical polishing on high gradients, in: V. Palmieri

(Ed.), Proceedings of the 8th Workshop on RF Superconductivity, Vol. I+II, INFN, Abano terme, 1997, pp. 759–813.
[5] K. Saito, et al., High gradient performance by electropolishing with 1300 MHz single and multi-cell niobium superconducting cavities, in: F. Krawcyk (Ed.), Proceedings of the 9th Workshop on RF Superconductivity, Vol. I+II, LANL, Santa Fe, 1999, pp. 288–291.
[6] E. Kako, K. Saito, et al., Improvement of cavity performance in the Saclay/Cornell/Desy's SC cavities, in: F. Krawcyk (Ed.), Proceedings of the 9th Workshop on RF Superconductivity, Vol. I+II, LANL, Santa Fe, 1999, pp. 179–186.
[7] L. Lilje, et al., Electropolishing and in-situ baking of 1.3 GHz niobium cavities, in: F. Krawcyk (Ed.), Proceedings of the 9th Workshop on RF Superconductivity, Vol. I+II, LANL, Santa Fe, 1999, pp. 74–76.
[8] L. Lilje, et al., Improved surface treatment of the superconducting TESLA cavities, Nucl. Instr. and Meth. A 516 (2–3) (2004) 213.
[9] L. Lilje, P. Schmüser, et al., Achievement of 35 MV/m in the superconducting nine-cell cavities for TESLA, Nucl. Instr. and Meth. A 524 (1–3) (2004) 1.
[10] J. Knobloch, et al., High field Q slope in SC cavities due to magnetic field enhancement at grain boundaries, in: F. Krawcyk (Ed.), Proceedings of the 9th Workshop on RF Superconductivity, Vol. I+II, LANL, Santa Fe, 1999, pp. 77–91.
[11] P. Kneisel, Preliminary experience with in-situ baking of niobium cavities, in: F. Krawcyk (Ed.), Proceedings of the 9th Workshop on RF Superconductivity, Vol. I+II, LANL, Santa Fe, 1999, pp. 328–335.
[12] P. Kneisel, Surface characterization: what has been done, what has been learned, SRF'03, Lübeck/Travemünde, September 2003.
[13] B. Visentin, Q-slope at high gradients: review about experiments and explanations, SRF'03, Lübeck/Travemünde, September 2003.
[14] G. Ciovati, P. Kneisel, G. Myneni, Effect of low temperature baking on niobium cavities, SRF'03, Lübeck/Travemünde, September 2003.
[15] J. Halbritter, RF residual losses, high electric and magnetic RF fields in superconducting cavities, in: L. Cifarelli, L. Maritato (Eds.), Superconducting Materials for High Energy Colliders, The Science and Culture Series—Physics, World Scientific, Singapore, 1999, pp. 59–79.
[16] We thank W. Gil (University of Hamburg) for these data.
[17] L. Lilje, Experimental investigations on superconducting niobium cavities at highest radiofrequency fields, DESY-PhDTHESIS-2001-034.
[18] E.H. Brandt, Superconductors in realistic geometries: geometric edge barrier versus pinning, Physica C 332 (2000) 99.
[19] D.K. Finnemore, T.F. Stromberg, C.A. Swenson, Superconducting properties of high-purity niobium, Phys. Rev. 149 (1966) 231.
[20] E. Maxwell, M. Strongin, Filamentary structure in superconductors, Phys. Rev. Lett. 10 (1963) 212.
[21] J.R. Clem, H.R. Kerchner, S.T. Sekula, AC permeability of defect-free type-II superconductors, Phys. Rev. 14 (1976) 1893.
[22] J. Kötzler, et al., Anisotropic dynamical scaling near the vortex-glass transition of twinned $YBa_2Cu_3O_{7-\delta}$, Phys. Rev. Lett. 72 (1994) 2081.
[23] E.H. Brandt, Superconductor disks and cylinders in an axial magnetic field: II. Non linear and linear AC susceptibilities, Phys. Rev. B 58 (1998) 6523.
[24] M. Tinkham, Effect of fluxoid quantization on transitions of superconducting films, Phys. Rev. 129 (1963) 2413.
[25] W. De Sorbo, Effect of dissolved gases on some superconducting properties of niobium, Phys. Rev. 134 (1964) A1119.
[26] A. Das Gupta, et al., Inhomogeneities in superconducting niobium surfaces, J. Appl. Phys. 47 (1976) 2146.
[27] D. Saint-James, P.G. de Gennes, Onset of superconductivity in decreasing fields, Phys. Lett. 7 (1963) 306.
[28] J.R. Hopkins, D.K. Finnemore, Surface superconductivity in niobium and niobium-tantalum alloys, Phys. Rev. B 9 (1974) 108.
[29] R.W. Rollins, J. Silcox, Nature of the AC transition in the superconducting surface sheath in Pb-2% In, Phys. Rev. 155 (1967) 404.
[30] A. Dacca, G. Gemme, L. Mattera, R. Parodi, XPS analysis of the surface composition of niobium for superconducting RF cavities, Appl. Surf. Sci. 126 (1998) 219.
[31] C.Z. Antoine, et al., Alternative approaches for surface treatment of Nb superconducting cavities, in: F. Krawcyk (Ed.), Proceedings of the 9th Workshop on RF Superconductivity, Vol. I+II, LANL, Santa Fe, 1999.
[32] K. Kowalski, XPS measurements at AGH on EP and BCP samples during 'in situ' bakeout, Private communication, 2001.
[33] C. Koch, J.O. Scarbrough, D. Kroeger, Effects of interstitial oxygen on the superconductivity of niobium, Phys. Rev. B 9 (1974) 888.
[34] V.V. Shmidt, in: V.V. Volkova, A.N. Chernov (Eds.), Physical Metallurgy, Physical Chemistry and Metals Physics of Superconductors, Nauka, Moscow, 1967, p. 90 (in Russian).
[35] L.P. Gor'kov, Theory of superconducting alloys in a strong magnetic field near the critical temperature, JETP 37 (1960) 998.
[36] J. Kötzler, L. von Sawilski, S. Casalbuoni, Evidence for a percolation-driven transition to coherent surface superconductivity, Phys. Rev. Lett. 92 (2004) 067005.
[37] P. Schmüser, Superconductivity in high energy particle accelerators, Prog. Nucl. Part. Phys. 49 (1) (2002), www.desy.de/~pschmues,supercon_acc.pdf.
[38] L. von Sawilski, S. Casalbuoni, J. Kötzler, Surface Superconductivity of Niobium: Onset of long-range coherence, SRF'03, Lübeck/Travemünde, September 2003.

[39] S. Casalbuoni, L. von Sawilski, J. Kötzler, Superconductivity above H_{c2} as a probe for Niobium RF-cavity surfaces, SRF'03, Lübeck/Travemünde, September 2003.
[40] J.P. Straley, Critical exponents for the conductivity of random resistor lattices, Phys. Rev. B 15 (1977) 5733.
[41] A.A. Abrikosov, Concerning surface superconductivity in strong magnetic fields, JETP 20 (1965) 480.
[42] H.J. Fink, L.J. Barnes, Critical state of the superconducting surface sheath, Phys. Rev. Lett. 15 (1965) 792.
[43] G. Deutscher, M.L. Rappaport, Critical currents of superconducting alluminium-germanium and lead-germanium thin film alloys near the metal-insulator transition, J. Phys. Lett. (Paris) 40 L (1979) 219.
[44] D. Hechtfischer, Temperaturabhängigkeit von Knightshift und Suszeptibilität von Vanadium und Niob, Z. Physik B 23 (1976) 255.
[45] R.J. Cava, et al., Antiferromagnetism and metallic conductivity in $Nb_{12}O_{29}$, Nature 350 (1991) 598; Electrical and magnetic properties of $Nb_2O_{5-\delta}$ crystallographic shear structures, Phys. Rev. B 44 (1991) 6973.
[46] J. Halbritter, private communication.